

Research Article

Open Access



Bioinspired cilia-based electronic skin for multimodal mechanical sensing via additive manufacturing

Jiangnan Yan^{1,2,#}, Jianing Ding^{1,2,#}, Yang Cao^{1,2,#}, Hongyu Yi^{1,2}, Limeng Zhan^{1,2}, Yifan Gao^{1,2}, Kongyu Ge^{1,2}, Hongjun Ji^{1,2}, Mingyu Li^{1,2}, Huanhuan Feng^{1,2,*}

¹Sauvage Laboratory for Smart Materials, Shenzhen Key Laboratory of Flexible Printed Electronics Technology, Harbin Institute of Technology, Shenzhen 518055, Guangdong, China.

²State Key Laboratory of Advanced Welding and Joining (Shenzhen), Harbin Institute of Technology, Shenzhen 518055, Guangdong, China.

[#]Authors contributed equally.

*Correspondence to: Dr. Huanhuan Feng, Sauvage Laboratory for Smart Materials, Shenzhen Key Laboratory of Flexible Printed Electronics Technology, Harbin Institute of Technology, Taoyuan Subdistrict, Nanshan District, Shenzhen 518055, Guangdong, China. E-mail: fenghuanhuan@hit.edu.cn

How to cite this article: Yan, J.; Ding, J.; Cao, Y.; Yi, H.; Zhan, L.; Gao, Y.; Ge, K.; Ji, H.; Li, M.; Feng, H. Bioinspired cilia-based electronic skin for multimodal mechanical sensing via additive manufacturing. *Soft Sci.* **2025**, *5*, 22. <https://dx.doi.org/10.20517/ss.2025.03>

Received: 12 Jan 2025 **First Decision:** 8 Feb 2025 **Revised:** 14 Feb 2025 **Accepted:** 27 Feb 2025 **Published:** 27 Apr 2025

Academic Editor: Huanyu Cheng **Copy Editor:** Pei-Yun Wang **Production Editor:** Pei-Yun Wang

Abstract

Electronic skin (e-skin) has been widely used in various fields such as health monitoring, robotic tactile perception, and bioinspired prosthetics due to its ability to detect a wide range of signals. However, traditional flexible e-skin is limited in providing detailed information about the sensing surface and the velocity of surface fluid motion, which restricts its further applications. In this study, we successfully fabricated a bioinspired cilia-based e-skin that enables the sensing and detection of surface morphology, Braille, and airflow velocity. The bioinspired cilia exhibited a linear sensing range for static detection, with bending angles from 15° to 60°, and a frequency range of 1-25 Hz for dynamic sensing. A single cilia could accurately detect surface morphology changes as small as 0.5 mm and recognize Braille characters. Additionally, the cilia-based e-skin was capable of sensing and detecting airflow velocity. This multifunctional cilia-based e-skin integrates three major functions: static tactile sensing (10-22,000 Pa), dynamic sliding sensing (0.8-5.4 cm/s), and airflow sensing (1.8-5.7 m/s). This advancement holds promise for providing a novel approach to the multifunctional integration of flexible electronics.

Keywords: Cilia-based e-skin, surface morphology detection, airflow velocity detection, multifunctional bionic integration



© The Author(s) 2025. **Open Access** This article is licensed under a Creative Commons Attribution 4.0 International License (<https://creativecommons.org/licenses/by/4.0/>), which permits unrestricted use, sharing, adaptation, distribution and reproduction in any medium or format, for any purpose, even commercially, as long as you give appropriate credit to the original author(s) and the source, provide a link to the Creative Commons license, and indicate if changes were made.



INTRODUCTION

In recent years, electronic skin (e-skin) has attracted increasing attention due to its significant potential in various fields, such as human-machine interfaces, health monitoring, and wearable devices^[1-13]. Its ability to maintain excellent performance on complex, curved surfaces makes it particularly promising^[14-20]. However, traditional e-skins face limitations in distinguishing surface protrusions and textures^[21-30], as well as in providing detailed and real-time information about the sensing surface. These constraints hinder their multifunctional integration in advanced applications.

Fish and arthropods such as crickets are exemplary animals that utilize cilia receptors for flow field perception^[31]. Scientists have conducted extensive and in-depth studies on the biological mechanisms of their cilia receptors^[32-35]. Inspired by the streamlined structures of fish^[31,36-39], researchers have incorporated cilia-like structures into e-skin to enhance the detection of surface morphology and fluid velocity. For example, Han *et al.*, inspired by the biological hair cells of fish, developed an artificial hair cell (AHC) flow sensor capable of accurately measuring the direction and speed of water flow^[40]. These cilia sensors, with their flexible and highly responsive hair-like structures, offer exceptional sensitivity in detecting surface features and fluid dynamics, making them invaluable for applications in human-machine interfaces.

Currently, flexible cilia structures are commonly fabricated using methods such as vertical demolding^[41-44], horizontal demolding^[45], and 3D printing^[41,46,47]. For instance, Ben *et al.* utilized a BMF S130 printer to create a cilia array mold, successfully fabricating cilia arrays with base diameters of 50 and 180 μm through vertical demolding^[43]. Takei *et al.* employed a horizontal cilia template, using polydimethylsiloxane (PDMS) curing and demolding to produce a flexible cilia structure^[45]. By integrating this structure with carbon nanotube (CNT)-silver nanoparticles (AgNPs) conductive materials, they achieved the detection of various surface morphologies. Fries *et al.* placed 3D-printed cilia structures on pre-fabricated flexible circuits, stabilizing them with a cross-shaped base structure and applying an additional PDMS layer for curing^[47]. The resulting flexible cilia sensor was effective for airflow detection. Among the various preparation methods, vertical demolding shows significant advantages in large-scale micro-cilia array preparation due to its ease of operation and complete cilia formation.

Leveraging the advantages of large-scale preparation based on vertical demolding, this study achieves multimodal perception synergy of static touch, dynamic sliding, and airflow speed through innovative biomimetic cilia structure design. Compared to traditional single-function sensor devices, the sensor system constructed in this work significantly improves in terms of functional integration, detection precision (0.5 mm), response sensitivity (0.4 s), and environmental adaptability. Specifically, the cilia sensor array prepared using the vertical demolding process exhibits a wide frequency detection characteristic of 1-25 Hz and excellent linear response within a bending angle range of 15°-60°. Functional validation demonstrates that this sensor can accurately identify complex surface morphologies, and its array integration further enables rapid interpretation of Braille characters. Notably, by simulating the functional partitioning mechanism of skin, the study innovatively integrates two-dimensional sensing units with cilia sensors to construct an e-skin system with differentiated functional characteristics. This integrated system successfully achieves real-time fusion and analysis of multiple physical quantities such as surface touch, sliding perception, and airflow monitoring, providing a new technological pathway for multifunctional integration of intelligent sensing systems.

EXPERIMENTAL

Materials

EGaIn (Shuochen, Changge, China), PDMS (Dow Corning, Midland, MI, USA), and Eco-flex-0030 (Smooth-On, Macungie, PA, USA) are utilized as the conductive functional material and packaging structural materials, respectively. NaOH (Damao, Tianjin, China) is used for the oxidation of EGaIn. Copper wires and weights for testing are purchased from the market.

Multifunctional bioinspired cilia-based e-skin fabrication

The fabrication process of the cilia-based e-skin is depicted in Figure 1. Initially, the P150 3D printer (Mofang, Chongqing, China) was utilized to print the pre-designed cilia template, circuit template and mold base. Each individual circuit sensor unit measured $3 \times 3 \text{ mm}^2$, with a line density of 32.0 cm^{-1} and a line width of 0.1 mm. Ecoflex was then applied to both the cilia and circuit templates with a coating thickness of 0.5 mm. The coated templates were heated at 45°C for one hour to cure, resulting in a flexible substrate with circuit patterns and conical-shaped flexible cilia. PDMS was coated onto the blank mold with a coating thickness of 1 mm, and was then heated at 45°C for 30 min to achieve a semi-cured film. Then, the flexible substrate, flexible cilia, and semi-cured PDMS film were bonded together, followed by heating at 45°C for two hours to ensure complete adhesion of the three components. Finally, oxidized EGaIn was injected into the circuit channels using a small syringe, and Cu wires were connected to the terminal ports and sealed using epoxy resin AB adhesive (with the A and B components pre-mixed in a 1:1 ratio for five minutes and then dried at 30°C for 5 h), resulting in the fabrication of a 2×3 modular cilia-based e-skin.

Performance testing of back-sensing units

In this experiment, the resistance response of back-sensing units to various loading conditions was measured using a multimeter with weight loading. To ensure uniform force distribution during loading, a thin gasket of $3 \times 3 \text{ mm}^2$ was pre-placed on the unit. To assess the linear sensing range and response time of the sensing units, weights of 0.005 g (5 Pa), 0.01 g (10 Pa), 0.05 g (55 Pa), 0.2 g (220 Pa), 1 g (1,100 Pa), 5 g (5,500 Pa), 20 g (22,000 Pa), and 50 g (55,000 Pa) were sequentially loaded onto and then removed from the sensing units to detect their response. To measure the pressure resolution of the sensing units, weights of 10, 5, 1, 0.2, 0.05, 0.01, and 0.005 g were incrementally added to the sensing units with a time interval of 100 s between additions, until no significant change in the resistance signal of the sensing unit was observed at the point of cumulative loading.

Experiment on optimization of cilia structural dimensions

This experiment measures the bending response of twelve cilia structures with different structural dimensions (four parameters for the cilia base diameter $D = 0.8, 1, 1.5, 2 \text{ mm}$, and three parameters for cilia length $H = 2.5, 3.5, 4.5 \text{ mm}$) to select the cilia structure with optimal performance. Four bending degrees of $15^\circ, 30^\circ, 45^\circ$, and 60° at the cilia tip were adopted. A multimeter was used to measure the resistance response of millimeter-scale cilia sensing units under these four bending conditions. To ensure consistent bending angles during the bending process, an angular scale was placed at the rear end of the cilia, and the operation was conducted under a microscope. A stepper motor was utilized to push the cilia tip to achieve a fixed bending angle. By analyzing the response time and resistance response magnitude of cilia of different sizes, the cilia dimensions with optimal performance were selected.

Performance testing and critical spacing study of cilia-based e-skin units

In this experiment, the resistance response of cilia-based sensing units to various bending degrees was measured using a multimeter by applying different levels of bending to the cilia tips. To ensure consistent bending degrees, an angular scale was placed at the rear end of the cilia, and a stepper motor was used to push the cilia tip to achieve a fixed bending angle. When measuring the angular sensing sensitivity and

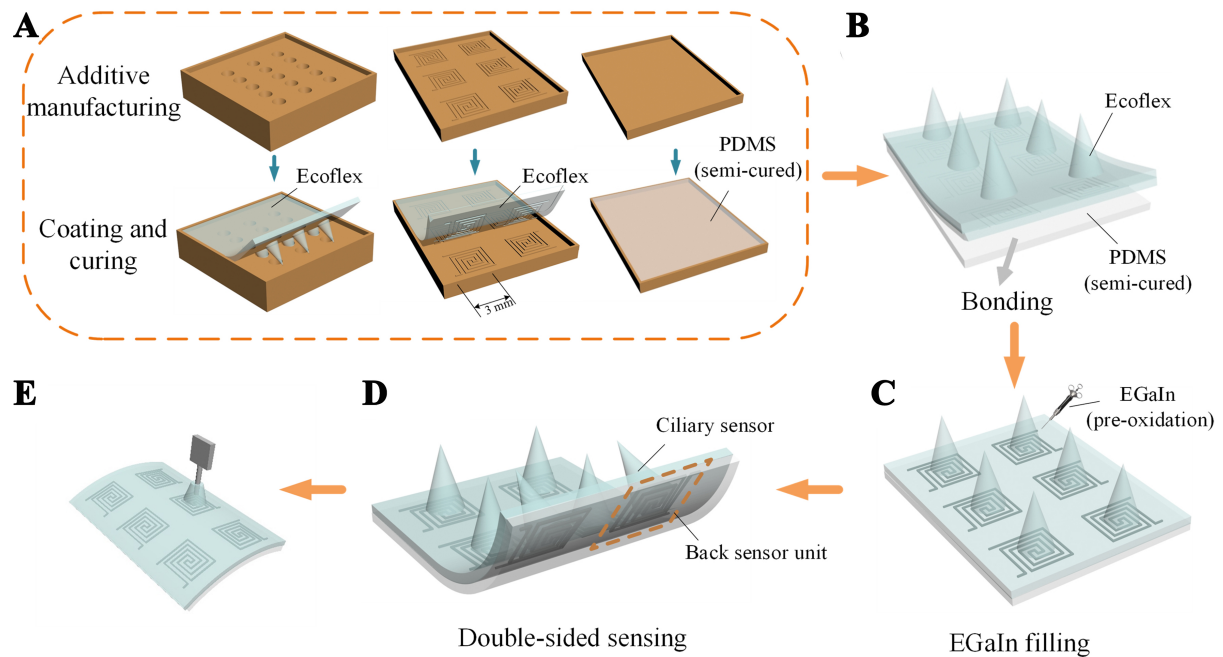


Figure 1. Fabrication process of cilia-based e-skin. (A) Created a flexible substrate with circuit patterns and conical cilia, along with a semi-cured PDMS film; (B) Bonded the flexible substrate, cilia, and semi-cured PDMS film together; (C) Injected oxidized EGaIn; (D) Implemented a double-sided sensing structure; (E) Integrated cilia with a rigid structure. e-skin: Electronic skin; PDMS: polydimethylsiloxane.

response time of the sensing units, the cilia tips were bent 15°, 30°, 45°, and 60° in the same direction and then returned to their unloaded state (with bending applied every ten seconds), while recording the resistance response magnitude and response time. To assess the frequency detection performance of the sensing units, a function generator was adjusted to output sine waves at 1, 2, 10, and 25 Hz, and a sinusoidal deformation load was applied to the surface of the sensing units by the front end of a vibration exciter. The response of the sensing units was obtained through the multimeter. To further integrate flexible cilia sensing arrays, the critical spacing between cilia sensing units needed to be determined. This was achieved by setting two different spacings of 1 and 2 mm between millimeter-scale cilia sensing units, applying bending to one of the sensing units, and observing the changes in resistance response of adjacent sensing units.

Rapid reading test of surface morphology and braille recognition using cilia-based e-skin

For the surface morphology test, modifications with different structures (tetrahedron, hexahedron, sphere) on a flat plate were designed using SolidWorks and printed using the BMF S130 printer (Boston Micro Fabrication, Shenzhen, China). The printed plate was then rinsed in anhydrous ethanol for five minutes, soaked in an anti-poisoning agent for five minutes, rinsed again in anhydrous ethanol for five minutes, and finally cured in an ultraviolet (UV) curing chamber for 12 h. The cilia-based e-skin was attached to a finger, and the cilia tips were used to contact the surface under test while moving at a constant speed. A multimeter was used to record the resistance response of the cilia-based e-skin.

For the Braille recognition test, raised Braille structures (hemispherical structures) were created on a flat plate using SolidWorks. Each Braille character consisted of six raised structures arranged in a 2 × 3 grid, with a spacing of 2 mm between columns and 4 mm between rows. The raised structures were hemispheres with a radius of 0.5 mm. The cilia-based e-skin was attached to a finger, and the cilia tips were used to contact the Braille under test while moving at a constant speed. A multichannel module of the multimeter

was utilized to detect the signal response from the cilia sensor array. By comparing the detected signals with a Braille chart, the recognition functionality of the system was tested.

RESULTS AND DISCUSSION

The fabrication process of the cilia-based e-skin is outlined in [Figure 1](#). First, the P150 3D printer prints the pre-designed cilia template, circuit template, and mold base. Ecoflex is applied to both templates, then heated at 45 °C for 1 h to create a flexible substrate with circuit patterns and conical cilia and PDMS is coated onto the blank mold and heated at 45 °C for 30 min to form a semi-cured film [[Figure 1A](#)]. The flexible substrate, cilia, and semi-cured PDMS film are bonded together and heated at 45 °C for 2 h to ensure complete adhesion [[Figure 1B](#)]. As shown in [Supplementary Figure 1](#), PDMS provides the necessary stiffness, while Ecoflex's high extensibility compensates for PDMS's low extensibility. After bonding, the composite exhibits a tensile strength of 1.92 MPa and an elongation at break of 400%.

Finally, oxidized EGeIn is injected into the circuit channels using a small syringe, and Cu wires are introduced [[Figure 1C](#)], completing the cilia-based e-skin.

Our e-skin boasts a dual-sided sensing structure, featuring a flat sensing array filled with EGeIn on its backside [[Figure 1D](#)], which offers sensing capabilities as detailed in [Supplementary Figure 2](#). This innovative skin can precisely deliver linear sensing across a load pressure range of 10 to 22,000 Pa, exhibiting a remarkably high-pressure resolution of 10 Pa and a swift response time of 0.14 s, thereby demonstrating exceptional pressure sensing performance. To enhance airflow sensitivity, a rigid structure is integrated into the cilia, as depicted in [Figure 1E](#). This system significantly improves airflow detection capability.

Based on this, we added a cilia structure to the front side of the e-skin to enhance its diverse sensing capabilities. To determine the optimal cilia sensing dimensions, we fabricated 12 different cilia structures using the demolding method and conducted performance tests on the e-skin equipped with these various cilia structures. The cilia structure parameters are shown in [Figure 2A](#), where the base diameter of the cilia was set at four different values ($D = 0.8, 1, 1.5, 2$ mm), and the cilia length was set at three different values ($H = 2.5, 3.5, 4.5$ mm). The fabricated cilia structures are illustrated in [Figure 2B-D](#).

To facilitate subsequent testing, we defined four bending angles (15°, 30°, 45°, 60°), as shown in [Figure 2E](#). We tested the sensitivity and response time of the 12 different cilia structures with these parameters. The detailed testing process is provided in [Supplementary Figure 3](#). The experimental results indicated that the cilia with a base diameter of $D = 2$ mm and a length of $H = 3.5$ mm exhibited the best performance, with a resistance change of 19 mΩ under a 60° bending condition and a response time of 0.4 s. This parameter was then selected for fabricating the cilia in the subsequent development of the e-skin.

Our e-skin can accurately detect the degree of cilia deformation and show a strong response to bending pressure loads. [Figure 3A](#) presents the resistance response data of the cilia-based e-skin at bending angles of 15°, 30°, 45°, and 60°. The data reveal a robust linear relationship between the resistance response values and the sine of the cilia bending angles within the 15°, 30°, 45°, and 60°, with a linear fit correlation coefficient R^2 exceeding 99%. The resistance increases due to cilia bending is approximately 1.17 mΩ at 15° and rises to 8.56 mΩ at 60°. Further analysis, shown in [Figure 3B](#), involved linear fitting of four sets of resistance response data. This demonstrates that our cilia-based e-skin effectively responds to bending actions within the 15°, 30°, 45°, and 60°, enabling the sensing and detection of various spatial signals. Additionally, [Figure 3C](#) illustrates the response times of the sensing units under different bending conditions. The

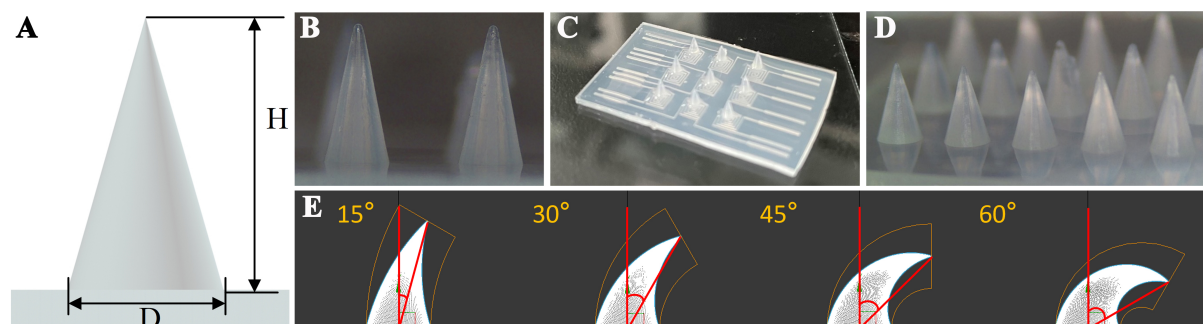


Figure 2. Cilia structure parameters and photographs. (A) Cilia structure parameters; (B) Photograph of cilia ($D = 2$ mm, $H = 3.5$ mm); (C) Photograph of cilia-based e-skin; (D) Photograph of cilia array; (E) Bending behavior of the cilia.

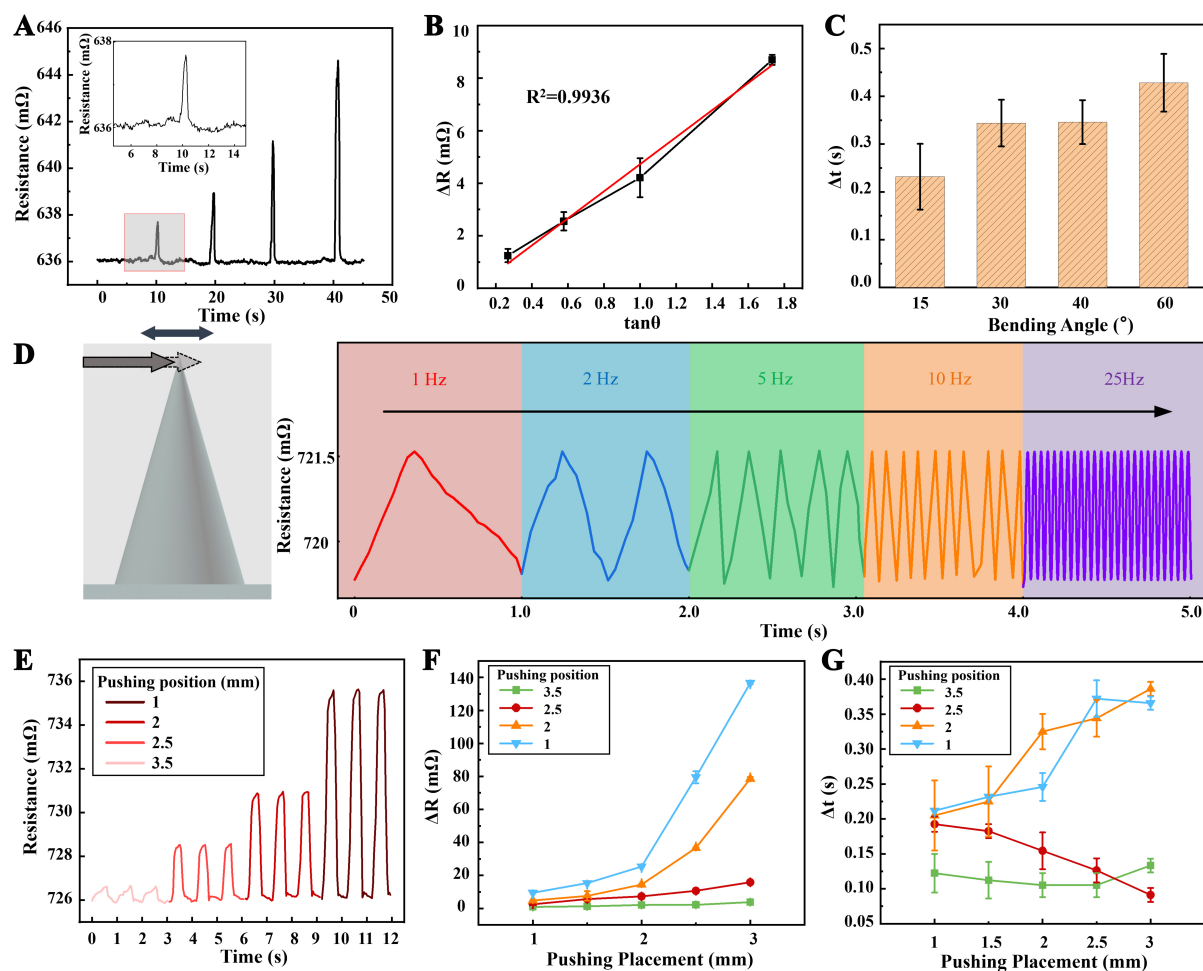


Figure 3. Performance test results of the cilia-based e-skin. (A) Resistance response of the cilia-based e-skin at bending angles of 15° , 30° , 45° , and 60° ; (B) Sine fitting results showing the relationship between response magnitude and bending angle; (C) Relationship between cilia bending angle and response time; (D) Frequency sensing range of the cilia; (E) Resistance response curves at different pushing positions; (F) Resistance response results for various pushing positions and distances; (G) Response time results for different pushing positions and distances. e-skin: Electronic skin.

response time increased from 0.2 to 0.4 s as the bending angle increased from 15° to 60° . This indicates that our cilia-based e-skin maintains extremely fast response times across varying bending degrees, ensuring

reliable performance under different pressure loads.

Additionally, our cilia-based e-skin demonstrates excellent wide-frequency detection capabilities. Using a frequency generator, we laterally pushed the tips of the cilia to test their ability to detect various input frequencies, as shown in [Figure 3D](#). The data indicate that the flexible cilia can effectively detect frequencies up to 25 Hz.

Furthermore, the conical flexible cilia are adept at accurately identifying the location of applied external bending pressure loads. We tested this capability by setting four positions (1, 2, 2.5, 3.5 mm) for the applied load, using a pushing machine to apply bending pressure loads at these positions. The pushing frequency was 1 Hz, and the pushing distance was 1 mm. The resulting resistance response curves are shown in [Figure 3E](#). The results reveal that, for the same magnitude of external pressure load, the cilia-based e-skin produces varying responses depending on the pushing position. As the pressure load's position approaches the substrate, the signal response increases. Specifically, when the pushing position is 1 mm from the substrate, the resistance response is approximately nine times greater compared to when the position is 3.5 mm.

Next, we investigated the signal response of the e-skin to different magnitudes of bending pressure loads. For the four pressure application positions, we used a pushing machine to set five different pushing distances and recorded the resistance response and response time of the e-skin, as shown in [Figure 3F](#) and [G](#). Regarding the resistance response, the overall slope of the resistance curve at pushing positions of 3.5 and 2.5 mm is relatively small, indicating that the signal response at these positions does not vary significantly with load magnitude. Conversely, at pushing positions of 2 and 1 mm, the signal response remains relatively constant when the pushing distance is less than 2 mm, with a slope similar to that at 3.5 and 2.5 mm. However, when the pushing distance exceeds 2 mm, the slope increases sharply. This is due to the increased tangential deformation of the base circuit as the cilia bend more, resulting in a dramatic rise in resistance response. For the response time, the magnitude of the load has minimal impact on response time at pushing positions of 3.5 and 2.5 mm, with little variation across the five pushing distances. In contrast, at pushing positions of 2 and 1 mm, the response time increases progressively with the pushing distance. This performance allows our cilia-based e-skin to effectively detect objects of varying depths and heights, demonstrating significant potential for detecting surface morphology and object shape.

Subsequently, we conducted a comprehensive evaluation of the overall performance of the cilia-based e-skin. Firstly, we established the minimum spacing between sensing units at 2 mm [[Supplementary Figure 4](#)], a critical parameter that enables the e-skin to accurately discern points separated by 2 mm, rivaling the resolution capability of human fingertips. To validate our cilia-based e-skin array multitouch functionality, we performed bending cilia experiments, with the specific experimental procedures outlined in [Supplementary Figure 5](#). By analyzing the response data from each sensing unit under three different loading conditions, we were able to precisely determine whether the cilia sensing units underwent bending. In instances where cilia bending occurred, we could also accurately identify the bending angle of each unit's cilia based on the response results, without any mutual interference among the cilia sensing units. This outcome indicates that our cilia-based e-skin array exhibits exceptional performance in multitouch cilia sensing. Furthermore, considering that flexible e-skin must adapt to various complex surfaces, we tested its performance in curved environments, as shown in [Supplementary Figure 6](#). The results demonstrate that our sensor maintains good linear sensing performance within the 15°-60° bending range, even on curved surfaces, thereby meeting the requirements for use on diverse curved geometries.

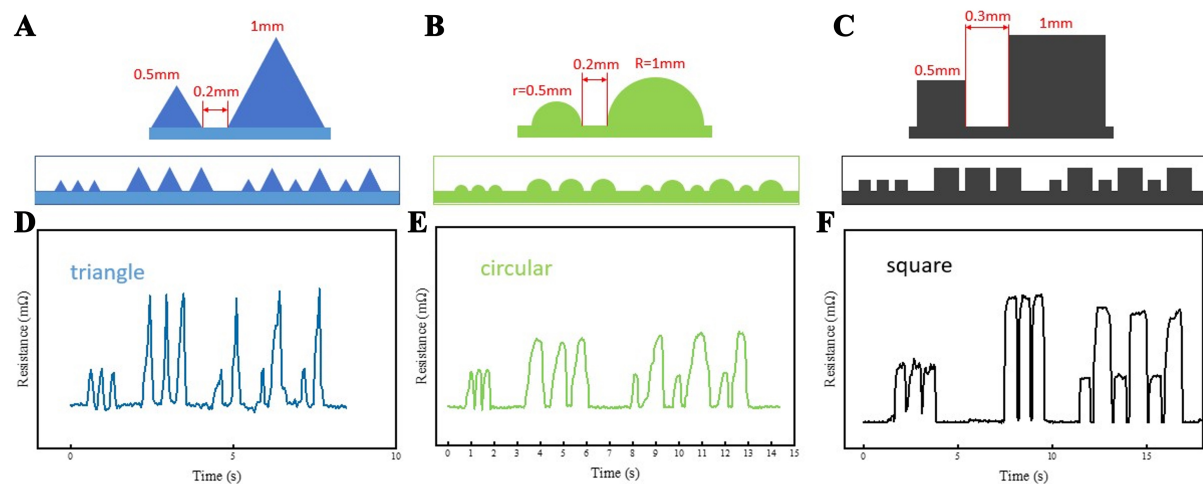


Figure 4. Surface morphology recognition schematic and resistance response curves. (A) Schematic diagrams of triangular; (B) Schematic diagrams of semicircular; (C) Schematic diagrams of square surface morphologies; (D) Resistance measurement curves corresponding to triangular; (E) Resistance measurement curves corresponding to semicircular; (F) Resistance measurement curves corresponding to square surface morphologies.

Our cilia-based e-skin demonstrates versatile applications. We first evaluated its capability to detect different surface morphologies. We printed three distinct surface morphology structures - triangular, semicircular, and square - with cross-sectional views shown in Figure 4A-C. These structures were placed on a flat surface, and the cilia sensing unit was uniformly pulled to ensure full contact between the cilia tips and all parts of the surface morphology structures. The resulting resistance response curves are shown in Figure 4D-F. The data clearly indicate that our cilia sensors can accurately detect surface morphologies of varying shapes and sizes. Additionally, the e-skin shows a linear change in signal response with varying heights. For instance, at a morphology height of 0.5 mm, the response magnitude is approximately half of that at a height of 1 mm. This allows for the determination of morphology height based on response curve values. Moreover, the shape of the response curve helps infer the type of morphology, enabling accurate identification of complex surface shapes. Overall, our cilia sensing units exhibit excellent performance in detecting and differentiating diverse surface morphologies.

Based on its precise detection of surface morphology, our cilia-based e-skin can accurately recognize millimeter-scale Braille. According to Braille standards, each Braille cell has a diameter of 1 mm and a height of 500 μm . We printed 2×3 Braille plates for the words “hello” and “HIT”. By using three cilia from the e-skin to contact the Braille plate and moving the sensor horizontally at a constant speed, the cilia passed sequentially over the hemispherical protrusions of the Braille plate. We measured the signal response of the cilia sensors with a multichannel digital multimeter, as shown in Figure 5A. Sensors 1, 2, and 3 detected the Braille symbols in the first, second, and third rows, respectively, with their resistance signal responses illustrated in Figure 5B. The signal peaks correspond to the maximum resistance response when the cilia are at the highest point of the Braille pattern. Each time the cilia traverse a Braille dot, the signal waveform changes. By comparing the signal responses from the three sensors with the Braille reference chart, we could accurately identify each Braille letter. As shown in Figure 5, we successfully recognized the lowercase “hello” and uppercase “HIT”, demonstrating the excellent capability of the e-skin for Braille letter recognition.

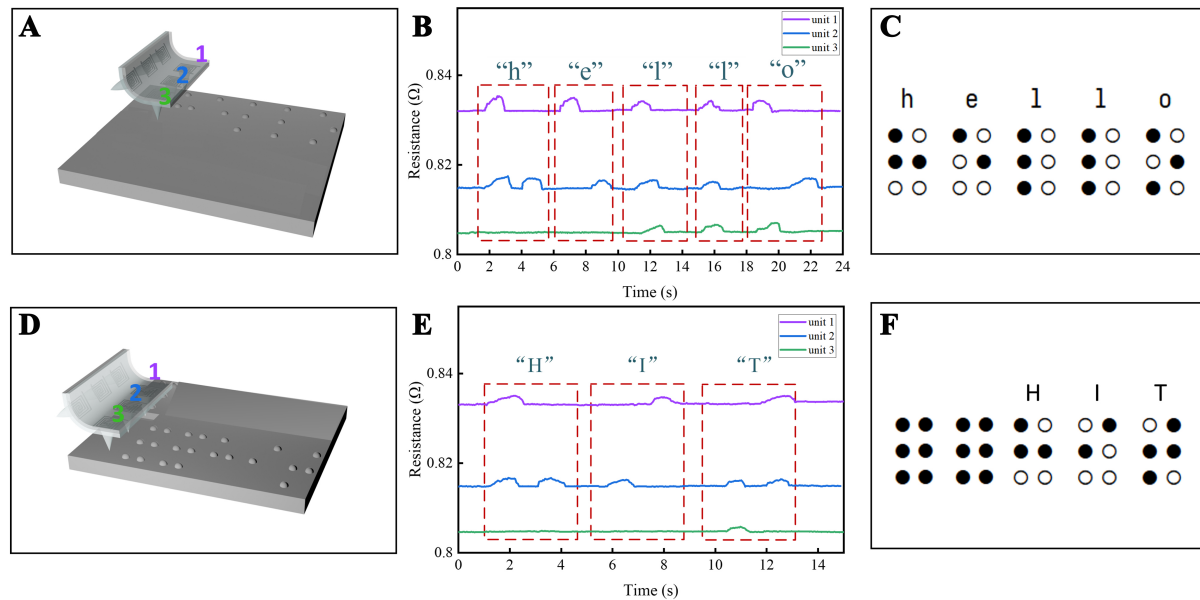


Figure 5. Braille recognition and sensor signal response. (A) Schematic diagram of Braille recognition; (B) Signal response of the sensing unit; (C) Braille reference chart for “hello”; (D) Schematic diagram of Braille recognition; (E) Signal response of the sensing unit; (F) Braille reference chart for “HIT”.

Due to the larger base diameter of our cilia, its sensitivity to airflow sensing was relatively low. To enhance airflow response sensitivity, we incorporated a “Click system” (a design that enhances airflow sensitivity through a rigid structure) into the cilia, introducing a rigid structure embedded within the flexible cilia base, as shown in [Supplementary Figure 7](#). This system significantly improved airflow detection capabilities. By leveraging the enhanced airflow performance of the cilia sensing units and the touch sensing capabilities of the sensor array, we attached the cilia-based e-skin to a fingertip, integrating the rigid-enhanced Click system into some of the cilia. This setup allowed the e-skin to simultaneously perform both airflow sensing and sliding touch control functions, as illustrated in [Figure 6](#). Color comparisons from the experiments reveal notable pressure differences. As shown in [Table 1](#), for single-point touch, the lowest pressure recorded was 1,200 Pa. In contrast, during a three-point touch scenario, sensor unit 1 experienced the peak pressure, reaching approximately 3,570 Pa. During the sliding experiment, the response results accurately followed our predefined sliding trajectory and indicated touch pressure throughout the process. As indicated in [Table 2](#), the pressure during sliding exceeded 3,000 Pa and remained relatively uniform throughout the entire movement. Additionally, during both multi-point touch and sliding touch experiments, we applied airflow. Analysis of the resistance response from sensor unit 4 allowed us to observe variations in airflow velocity, which closely matched the actual wind speed applied.

This comprehensive experimental study, which combines multi-point touch, sliding touch, and airflow sensing, demonstrates that the cilia-based e-skin can effectively achieve trajectory recognition, pressure detection, and airflow sensing in curved environments. This showcases its significant potential for multifunctional integrated bionic e-skin applications.

CONCLUSIONS

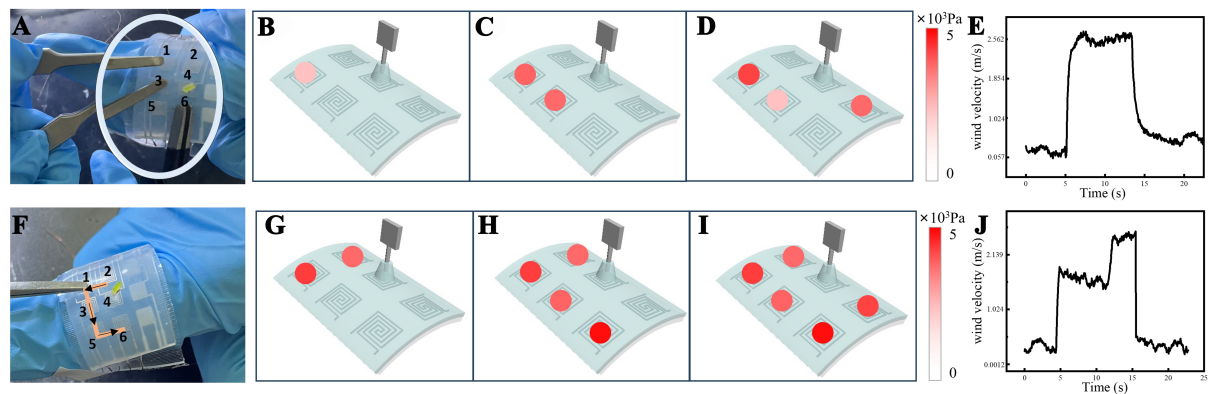
In this study, we successfully developed a bionic cilia-based e-skin utilizing gallium-based liquid metal and a flexible substrate, enabling multifunctional sensing capabilities. This cilia-based e-skin can measure pressures from 10 to 22,000 Pa, with a maximum response time of just 0.14 s. This is significantly superior

Table 1. Pressure values for multi-point touch on the bionic nose tip model ($\times 10^3$ Pa)

Unit	b	c	d
1	1.20	2.54	3.57
3	-	2.14	1.13
6	-	-	2.10

Table 2. Pressure values for sliding test on the bionic nose tip model ($\times 10^3$ Pa)

Unit	g	h	i
1	3.69	3.69	3.69
2	3.14	3.14	3.14
3	-	3.12	3.12
4	-	-	-
5	-	4.23	4.23
6	-	3.47	3.47

**Figure 6.** Performance testing of cilia-based e-skin. (A-E) Photographs and response results for multi-point touch and airflow sensing using the cilia-based e-skin; (F and G) Photographs and response results for sliding sensing and airflow sensing using the cilia-based e-skin. e-skin: Electronic skin.

to the flexible e-skin technologies recently reported (such as the CNT-based sensor in reference^[9] with a response time of 0.3 s). The cilia exhibit linear sensing across a bending range of 15° to 60° and can detect frequencies from 1 to 25 Hz, which covers the main low-frequency range of human tactile perception (0.4–500 Hz) and extends the high-frequency detection capability compared to existing biomimetic cilia sensors. Our cilia-based e-skin can detect objects at various depths and heights, accurately recognizing complex surface morphologies, and precisely identifying millimeter-scale Braille, showcasing exceptional performance in surface morphology sensing.

Moreover, by incorporating a “rigid-enhanced Click system” into the cilia, we enhanced the sensitivity of airflow detection. The integrated system enables the e-skin to perform static touch sensing (10–22,000 Pa), dynamic sliding sensing (0.8–5.4 cm/s), and airflow sensing (1.8–5.7 m/s), demonstrating its potential for multifunctional integration in flexible electronics applications.

DECLARATIONS

Authors' contributions

Data curation, formal analysis, investigation, methodology, writing original draft: Yan, J.; Ding, J.; Yi, H.; Cao, Y.; Zhan, L.

Data analysis and interpretation: Yi, H.; Cao, Y.; Zhan, L.

Visualization: Gao, Y.; Ge, K.

Conceptualization, funding acquisition, project administration, resources, supervision: Ji, H.; Li, M.; Feng, H.

Availability of data and materials

The authors declare that the primary data supporting the findings of this study are available within the paper and its [Supplementary Materials](#). Additional data are available from the corresponding authors upon reasonable request.

Financial support and sponsorship

This work was financially supported by the Shenzhen Science and Technology Planning Project (grant Nos. JCYJ20180507183224565 and ZDSYS20190902093220279) and Shenzhen Peacock Group (grant Nos. KQTD20170809110344233 and KQTD20200820113045083).

Conflicts of interest

All authors declared that there are no conflicts of interest.

Ethical approval and consent to participate

Not applicable.

Consent for publication

Not applicable.

Copyright

© The Author(s) 2025.

REFERENCES

1. Jian, M.; Wang, C.; Wang, Q.; et al. Advanced carbon materials for flexible and wearable sensors. *Sci. China. Mater.* **2017**, *60*, 1026-62. [DOI](#)
2. Chen, J.; Zhu, Y.; Chang, X.; et al. Recent progress in essential functions of soft electronic skin. *Adv. Funct. Mater.* **2021**, *31*, 2104686. [DOI](#)
3. Nie, B.; Liu, S.; Qu, Q.; Zhang, Y.; Zhao, M.; Liu, J. Bio-inspired flexible electronics for smart E-skin. *Acta. Biomater.* **2022**, *139*, 280-95. [DOI](#)
4. Bingger, P.; Zens, M.; Woias, P. Highly flexible capacitive strain gauge for continuous long-term blood pressure monitoring. *Biomed. Microdevices.* **2012**, *14*, 573-81. [DOI](#) [PubMed](#)
5. Gao, W.; Ota, H.; Kiriya, D.; Takei, K.; Javey, A. Flexible electronics toward wearable sensing. *Acc. Chem. Res.* **2019**, *52*, 523-33. [DOI](#) [PubMed](#)
6. Yilmaz, T.; Foster, R.; Hao, Y. Detecting vital signs with wearable wireless sensors. *Sensors* **2010**, *10*, 10837-62. [DOI](#) [PubMed](#) [PMC](#)
7. Amjadi, M.; Pichitpajongkit, A.; Lee, S.; Ryu, S.; Park, I. Highly stretchable and sensitive strain sensor based on silver nanowire-elastomer nanocomposite. *ACS. Nano.* **2014**, *8*, 5154-63. [DOI](#) [PubMed](#)
8. Wang, Y.; Tebyetekerwa, M.; Liu, Y.; et al. Extremely stretchable and healable ionic conductive hydrogels fabricated by surface competitive coordination for human-motion detection. *Chem. Eng. J.* **2021**, *420*, 127637. [DOI](#)
9. Li, S.; Liu, G.; Wen, H.; et al. A Skin-like pressure- and vibration-sensitive tactile sensor based on polyacrylamide/silk fibroin elastomer. *Adv. Funct. Mater.* **2022**, *32*, 2111747. [DOI](#)
10. Hou, C.; Tai, G.; Liu, Y.; Wu, Z.; Liang, X.; Liu, X. Borophene-based materials for energy, sensors and information storage applications. *Nano. Res. Energy.* **2023**, *2*, e9120051. [DOI](#)

11. Zhou, Y.; Wang, Q.; Zhang, X.; et al. Piezoionic transfer effect in topological borophene-bismuthene derivative micro-leaves for robust supercapacitive electronic skins. *Nano. Energy*. **2022**, *104*, 107970. DOI
12. Zeng, Y.; Qin, Y.; Yang, Y.; Lu, X. A low-cost flexible capacitive pressure sensor for health detection. *IEEE. Sensors. J.* **2022**, *22*, 7665-73. DOI
13. Yang, X.; Chen, S.; Shi, Y.; Fu, Z.; Zhou, B. A flexible highly sensitive capacitive pressure sensor. *Sens. Actuators. A. Phys.* **2021**, *324*, 112629. DOI
14. Yang, L.; Wang, H.; Yuan, W.; et al. Wearable pressure sensors based on MXene/tissue papers for wireless human health monitoring. *ACS. Appl. Mater. Interfaces*. **2021**, *13*, 60531-43. DOI
15. Cai, Y.; Shen, J.; Yang, C. W.; et al. Mixed-dimensional MXene-hydrogel heterostructures for electronic skin sensors with ultrabroad working range. *Sci. Adv.* **2020**, *6*, eabb5367. DOI PubMed PMC
16. Gao, Y.; Ota, H.; Schaler, E. W.; et al. Wearable microfluidic diaphragm pressure sensor for health and tactile touch monitoring. *Adv. Mater.* **2017**, *29*, 1701985. DOI PubMed
17. Jia, J.; Huang, G.; Deng, J.; Pan, K. Skin-inspired flexible and high-sensitivity pressure sensors based on rGO films with continuous-gradient wrinkles. *Nanoscale* **2019**, *11*, 4258-66. DOI
18. Zhan, L.; Cao, Y.; Gao, Y.; et al. Additively fabricated electronic skin with high performance in dynamic sensing as human skin. *ACS. Appl. Electron. Mater.* **2023**, *5*, 2017-25. DOI
19. Zhang, H.; Li, H.; Li, Y. Biomimetic electronic skin for robots aiming at superior dynamic-static perception and material cognition based on triboelectric-piezoresistive effects. *Nano. Lett.* **2024**, *24*, 4002-11. DOI
20. Feng, H.; Liu, Y.; Feng, L.; et al. Additively manufactured flexible electronics with ultrabroad range and high sensitivity for multiple physiological signals' detection. *Research* **2022**, *2022*, 9871489. DOI PubMed PMC
21. Liu, C. H.; Yu, X. Silver nanowire-based transparent, flexible, and conductive thin film. *Nanoscale. Res. Lett.* **2011**, *6*, 75. DOI PubMed PMC
22. Mehta, R.; Chugh, S.; Chen, Z. Enhanced electrical and thermal conduction in graphene-encapsulated copper nanowires. *Nano. Lett.* **2015**, *15*, 2024-30. DOI PubMed
23. Wissman, J. P.; Sampath, K.; Freeman, S. E.; Rohde, C. A. Capacitive bio-inspired flow sensing cupula. *Sensors* **2019**, *19*, 2639. DOI
24. Slinker, K. A.; Kondash, C.; Dickinson, B. T.; Baur, J. W. CNT-based artificial hair sensors for predictable boundary layer air flow sensing. *Adv. Mater. Technol.* **2016**, *1*, 1600176. DOI
25. Huang, S.; Zhang, B.; Lin, Y.; Lee, C. S.; Zhang, X. Compact biomimetic hair sensors based on single silicon nanowires for ultrafast and highly-sensitive airflow detection. *Nano. Lett.* **2021**, *21*, 4684-91. DOI
26. Abolpour Moshizi, S.; Azadi, S.; Belford, A.; et al. Development of an ultra-sensitive and flexible piezoresistive flow sensor using vertical graphene nanosheets. *Nanomicro. Lett.* **2020**, *12*, 109. DOI PubMed PMC
27. Niu, H.; Li, H.; Gao, S.; et al. Perception-to-cognition tactile sensing based on artificial-intelligence-motivated human full-skin bionic electronic skin. *Adv. Mater.* **2022**, *34*, e2202622. DOI
28. Kim, K. H.; Kim, J. H.; Ko, Y. J.; Lee, H. E. Body-attachable multifunctional electronic skins for bio-signal monitoring and therapeutic applications. *Soft. Sci.* **2024**, *4*, 24. DOI
29. Neto, J.; Chirila, R.; Dahiya, A. S.; Christou, A.; Shakthivel, D.; Dahiya, R. Skin-inspired thermoreceptors-based electronic skin for biomimicking thermal pain reflexes. *Adv. Sci.* **2022**, *9*, e2201525. DOI PubMed PMC
30. Ahmadi, H.; Moradi, H.; Pastras, C. J.; Moshizi, S. A.; Wu, S.; Asadnia, M. Development of ultrasensitive biomimetic auditory hair cells based on piezoresistive hydrogel nanocomposites. *ACS. Appl. Mater. Interfaces*. **2021**, *13*, 44904-15. DOI PubMed
31. Rizzi, F.; Qualtieri, A.; Dattoma, T.; Epifani, G.; De Vittorio, M. Biomimetics of underwater hair cell sensing. *Microelectron. Eng.* **2015**, *132*, 90-7. DOI
32. Shizhe, T. Underwater artificial lateral line flow sensors. *Microsyst. Technol.* **2014**, *20*, 2123-36. DOI
33. Goulet, J.; Engelmann, J.; Chagnaud, B. P.; Franosch, J. M. P.; Suttner, M. D.; van Hemmen, J. L. Object localization through the lateral line system of fish: theory and experiment. *J. Comp. Physiol. A. Neuroethol. Sens. Neural. Behav. Physiol.* **2008**, *194*, 1-17. DOI PubMed
34. Klein, A.; Bleckmann, H. Determination of object position, vortex shedding frequency and flow velocity using artificial lateral line canals. *Beilstein. J. Nanotechnol.* **2011**, *2*, 276-83. DOI PubMed PMC
35. Dangles, O.; Magal, C.; Pierre, D.; Olivier, A.; Casas, J. Variation in morphology and performance of predator-sensing system in wild cricket populations. *J. Exp. Biol.* **2005**, *208*, 461-8. DOI PubMed
36. Ozaki, Y.; Ohyama, T.; Yasuda, T.; Shimoyama, I. An air flow sensor modeled on wind receptor hairs of insects. In: *Proceedings IEEE Thirteenth Annual International Conference on Micro Electro Mechanical Systems (Cat. No.00CH36308*, Miyazaki, Japan. Jan 23-27, 2000. IEEE, 2022; pp. 531-6. DOI
37. Fan, Z.; Chen, J.; Zou, J.; Bullen, D.; Liu, C.; Delcomyn, F. Design and fabrication of artificial lateral line flow sensors. *J. Micromech. Microeng.* **2002**, *12*, 655. DOI
38. Yang, Y.; Klein, A.; Bleckmann, H.; Liu, C. Artificial lateral line canal for hydrodynamic detection. *Appl. Phys. Lett.* **2011**, *99*, 023701. DOI
39. Wang, Y. H.; Lee, C. Y.; Chiang, C. M. A MEMS-based air flow sensor with a free-standing microcantilever structure. *Sensors* **2007**, *7*, 2389-401. DOI
40. Han, J. S.; Oh, K. H.; Moon, W. K.; et al. Bio-inspired piezoelectric artificial hair cell sensor fabricated by powder injection molding.

- Smart. Mater. Struct.* **2015**, *24*, 125025. DOI
41. Wakabayashi, S.; Yamaguchi, T.; Arie, T.; Akita, S.; Takei, K. Out-of-plane flexible electronic whisker array. In: *2020 IEEE 33rd International Conference on Micro Electro Mechanical Systems (MEMS)*, Vancouver, Canada. Jan 18-22, 2020. IEEE, 2020; pp. 235-8. DOI
 42. Liu, G.; Jiang, Y.; Wu, P.; Ma, Z.; Chen, H.; Zhang, D. Artificial whisker sensor with undulated morphology and self-spread piezoresistors for diverse flow analyses. *Soft. Robot.* **2023**, *10*, 97-105. DOI
 43. Ben, S.; Yao, J.; Ning, Y.; et al. A bioinspired magnetic responsive cilia array surface for microspheres underwater directional transport. *Sci. China. Chem.* **2020**, *63*, 347-53. DOI
 44. An, H.; Wang, S.; Li, D.; Peng, Z.; Chen, S. Self-cleaning performance of the micropillar-arrayed surface and its micro-scale mechanical mechanism. *Langmuir* **2021**, *37*, 10079-88. DOI
 45. Takei, K.; Yu, Z.; Zheng, M.; Ota, H.; Takahashi, T.; Javey, A. Highly sensitive electronic whiskers based on patterned carbon nanotube and silver nanoparticle composite films. *Proc. Natl. Acad. Sci. U. S. A.* **2014**, *111*, 1703-7. DOI PubMed PMC
 46. Wu, Z.; Ai, J.; Ma, Z.; et al. Flexible out-of-plane wind sensors with a self-powered feature inspired by fine hairs of the spider. *ACS. Appl. Mater. Interfaces.* **2019**, *11*, 44865-73. DOI
 47. Fries, F.; Valdivia y Alvarado, P. Whisker-like sensors with soft resistive follicles. In: *2017 IEEE International Conference on Robotics and Biomimetics (ROBIO)*, Macau. Dec 05-08, 2017. IEEE, 2017; pp. 2038-43. DOI